Journal of Experimental Botany, Vol. 71, No. 22 pp. 7286–7300, 2020
doi:10.1093/jxb/eraa392 Advance Access Publication 11 December 2020

RESEARCH PAPER

Coordinated decline of leaf hydraulic and stomatal conductances under drought is not linked to leaf xylem embolism for different grapevine cultivars

Caetano Albuquerque[1], Christine Scoffoni[2], Craig R. Brodersen[3], Thomas N. Buckley[4], Lawren Sack[5] and Andrew J. McElrone[1,6,*]

[1] Department of Viticulture and Enology, University of California, Davis, 595 Hilgard Lane, Davis, CA 95616, USA
[2] Department of Biological Sciences, California State University, Los Angeles, 5151 State University Drive, Los Angeles, CA 90032, USA
[3] School of the Environment, Yale University, 195 Prospect Street, New Haven, CT 06511, USA
[4] Department of Plant Sciences, University of California, Davis, One Shields Avenue, Davis, CA 95616, USA
[5] Department of Ecology and Evolutionary Biology, University of California Los Angeles, 621 Charles E. Young Drive South, Los Angeles, CA, 90095, USA
[6] USDA-Agricultural Research Service, Davis, CA 95616, USA

* Correspondence: ajmcelrone@ucdavis.edu or andrew.mcelrone@usda.gov

Received 21 April 2020; Editorial decision 18 August 2020; Accepted 27 October 2020

Editor: Tracy Lawson, University of Essex, UK

Abstract

Drought decreases water transport capacity of leaves and limits gas exchange, which involves reduced leaf leaf hydraulic conductance (K_{leaf}) in both the xylem and outside-xylem pathways. Some literature suggests that grapevines are hyper-susceptible to drought-induced xylem embolism. We combined K_{leaf} and gas exchange measurements, micro-computed tomography of intact leaves, and spatially explicit modeling of the outside-xylem pathways to evaluate the role of vein embolism and K_{leaf} in the responses of two different grapevine cultivars to drought. Cabernet Sauvignon and Chardonnay exhibited similar vulnerabilities of K_{leaf} and g_s to dehydration, decreasing substantially prior to leaf xylem embolism. K_{leaf} and g_s decreased by 80% for both cultivars by Ψ_{leaf} approximately –0.7 MPa and –1.2 MPa, respectively, while leaf xylem embolism initiated around Ψ_{leaf} = –1.25 MPa in the midribs and little to no embolism was detected in minor veins even under severe dehydration for both cultivars. Modeling results indicated that reduced membrane permeability associated with a Casparian-like band in the leaf vein bundle sheath would explain declines in K_{leaf} of both cultivars. We conclude that during moderate water stress, changes in the outside-xylem pathways, rather than xylem embolism, are responsible for reduced K_{leaf} and g_s. Understanding this mechanism could help to ensure adequate carbon capture and crop performance under drought.

Keywords: Anatomy, drought, ecophysiology, gas exchange, leaf hydraulics, micro-CT, modeling, *Vitis*.

Introduction

Grapes are an economically important and widely cultivated crop worldwide, but vineyards that produce premium wine are most commonly located in regions characterized by dry and hot summers. Climate change is predicted to have a major impact on wine grape production due in part to increased crop water demands associated with higher

evapotranspiration and increased water scarcity in arid growing regions (Diffenbaugh and Scherer, 2013; Hannah *et al.*, 2013). Deficit irrigation strategies that purposefully induce water stress are also commonly used to control grapevine vigor and improve fruit quality. Wine grape cultivars exhibit contrasting responses to drought, which influences cultivar selection that will be a key factor for wine grape growing in a changing climate (Morales-Castilla *et al.*, 2020). Cabernet Sauvignon (red wine grape) and Chardonnay (white wine grape) are the two most widely cultivated wine grapes worldwide, and are grown in contrasting environmental conditions. A better understanding of how water stress-induced changes in hydraulic traits impact grapevine physiology could help to predict tolerance of given cultivars in future climatic conditions.

Leaf-level mechanisms are hypothesized to play an important role in the differential responses of grapevine cultivars to drought (Schultz, 2003). Grapevines exhibit long and wide xylem conduits that can extend from stems to leaf tips (Chatelet *et al.*, 2006; Thorne *et al.*, 2006), exacerbating the threat of hydraulic dysfunction due to water stress. Once water leaves the petiole, it flows through the veins from the lower to higher orders, finally reaching the free-ending veins in the leaf areole while also leaking radially across all veins along the way (Sack and Holbrook, 2006). To enter the outside-xylem pathways, water crosses the bundle sheath (BS) and flows across the mesophyll cells, evaporating into the intercellular airspace, and finally diffusing out of the stomata to the atmosphere (Rockwell *et al.*, 2014; Buckley *et al.*, 2017; Scoffoni *et al.*, 2017*b*). Declining leaf hydraulic conductance (K_{leaf}) under drought stress can be driven not only by reduced xylem hydraulic conductance (K_x) but also by reduced outside-xylem hydraulic conductance (K_{ox}).

Declines in K_{leaf} and stomatal conductance (g_s) during drought have been largely attributed to xylem embolism formation in several species including grapevines (Salleo *et al.*, 2000; Nardini *et al.*, 2001, 2003; Bucci *et al.*, 2003; Trifilò *et al.*, 2003a, b; Brodribb and Holbrook, 2004; Zufferey *et al.*, 2011; Johnson *et al.*, 2009, 2012). Similarly, a strong link between petiole xylem embolism and drought-induced leaf death was recently found in avocado trees (Cardoso *et al.*, 2020), and Lovisolo *et al.* (2008) found that grapevine petioles lost ~80% of their hydraulic conductance due to embolism at leaf water potentials (Ψ_{leaf}) of −1.4 MPa, but these results were obtained with hydraulic methods on excised leaves that have recently been questioned (e.g. McElrone *et al.*, 2012; Torres-Ruiz *et al.*, 2015). Hochberg *et al.* (2017*a*, 2019) used an optical method to examine embolism spread in grapevine leaves under drought, and found xylem to be more resistant to embolism than previous studies. Recent work in several other species from different ecological backgrounds showed that leaf veins are extremely resistant to drought-induced embolism formation and pointed towards the outside-xylem pathways as the driver of declines in K_{leaf} and g_s during initial stages of water stress (Scoffoni *et al.*, 2017*a*, *b*, 2018). Trifilò *et al.* (2016) found that the relative contribution of xylem versus outside-xylem pathways to declining K_{leaf} is species-specific across several studied species, but found also that both pathways contribute equally in a grapevine species. Direct measures of K_{leaf} combined with high-resolution visualization of embolism in intact leaves would help to further resolve their respective roles in hydraulic decline and their role in stomatal closure under drought stress. Work is needed to resolve incongruences in previous findings on grapevine in particular, given its central role in ongoing debates within the plant hydraulics community.

Here, we compared leaf-level responses of *Vitis vinifera* L. cvs 'Cabernet Sauvignon' and 'Chardonnay' wine grapes to drought stress; the former is largely grown in warmer and drier regions, whereas the latter is more commonly cultivated in cooler, humid climates. In 2019, these two cultivars alone accounted for >39% of the cultivated wine grape acreage in California, which leads US production at ~85% of the country's total. We used a combination of high-resolution X-ray micro-computed tomography (microCT) of intact leaves on potted plants subjected to different water potentials, light microscopy for anatomical comparisons, and physiological measurements such as K_{leaf}, g_s, and turgor loss point to clarify the role of xylem embolism in grape leaves during dehydration. We also used a spatially explicit model of water transport outside-xylem (MOFLO 2.0; Buckley *et al.*, 2017; Scoffoni *et al.*, 2018) to elucidate the anatomical drivers of K_{leaf} during dehydration.

Materials and methods

Plant material

Own-rooted *V. vinifera* L. cvs 'Cabernet Sauvignon' and 'Chardonnay' propagated from woody cuttings were obtained from the Foundation Plant Services (FPS, Davis, CA, USA) and grown in a greenhouse at the University of California, Davis. Greenhouse temperature was maintained between 16 °C and 32 °C, with a photoperiod of 15/9 h using supplemental light to maintain a stable photoperiod and a relative humidity of 40–80%. Plants were grown in 1.5 liter pots with a soil composed of 40% washed sand, 20% sphagnum peat moss, 20% redwood compost, and 20% pumice rock. Plants were irrigated daily with a diluted fertilized solution to maintain well-watered status, thus ensuring that they were grown in the same conditions.

X-ray micro-computed tomography

Leaves still attached to intact plants were scanned with high-resolution X-ray microCT imaging at the Lawrence Berkeley National Laboratory Advanced Light Source (ALS; Beamline 8.3.2) in July and August 2015. Each sample was scanned in the midrib, targeting the first branching of secondary veins after the petiole–lamina junction (see Supplementary Fig. S1 at *JXB* online). This location was chosen due to the importance of major veins for leaf hydraulics and function (Sack *et al.*, 2003), especially in the basal portions of the leaf, so all midrib xylem conduits would be scanned before branching of conduits to secondary veins. Plants were allowed to naturally dehydrate in the greenhouse by discontinuing irrigation before being taken to the ALS, to achieve a range of water potentials. At the ALS, a leaf located a maximum of three nodes below the scanned leaf was sealed in a plastic bag lined with aluminum foil for at least 20 min to minimize transpiration and equilibrate the leaf with stem water potential, which was then measured with a pressure chamber (Plant Moisture Stress, Model 1000, Albany, OR, USA). The range of water potentials used in this study was between Ψ_w= −0.3 MPa and Ψ_w= −2 MPa, which is similar to values grapevines usually experience between Ψ_w= −0.3 and Ψ_w= −1.8 MPa in the field (Choat *et al.*, 2010; Charrier *et al.*, 2018). Levels of water stress have been previously defined by Smith and Prichard (2002) for several field-grown winegrape cultivars as: no stress Ψ_w> −1 MPa; mild −1 MPa>Ψ_w> −1.2 MPa; moderate

–1.2 MPa<Ψ_w< –1.4 MPa; and severe stress Ψ_w< –1.6 MPa. A total of 22 samples of Cabernet Sauvignon ranging from Ψ_w= –0.1 MPa to Ψ_w= –2.8 MPa and 19 of Chardonnay spanning from Ψ_w= –0.2 MPa to Ψ_w= –2.9 MPa were taken. A subset of samples were used to evaluate embolism in all veins and tissues dimensions within the scanned field of view (FOV), which was on average 3.89 mm^2 (± 0.15 SE, n=23). The pot was then bagged to maintain the plant at this water status to prepare the plants to be scanned. We then fixed a 2 mm copper wire to the leaf midrib with a piece of Kapton tape (DuPont, Wilmington, DE, USA). This wire served as an X-ray-dense reference point during the initial image preparation process to center the midrib in the middle of the FOV (Suppplementary Fig. S1). The leaf still attached to the intact plant was then placed between two half-cylinder pieces of styrofoam to be fixed in the center of the stage and the whole plant was placed inside a 9 cm diameter custom-made plexiglass cylinder. The plant and cylinder were then attached to the scanning stage. After centering the sample in the stage using the copper wire reference, the scan was performed between 10 min and 15 min depending on the area scanned. One single scan was performed per plant to eliminate potential effects associated with repeated X-ray scans on this soft tissue. The energy used was between 19 keV and 23 keV, and 1024 projection images were taken in continuous tomography mode, resulting in images with 1.27 μm^3 voxel resolution.

Image analysis for embolism quantification

The resulting 2D projection images were then reconstructed in 3D in Fiji (FIJI-ImageJ version 1.46r; National Institutes of Health) using a custom plugin that utilizes Octopus 8.3 (Institute for Nuclear Sciences, University of Ghent, Belgium) to create a stack of images. The resulting image stacks were then evaluated in the transverse plane using Fiji to determine the presence of air-filled vessels in the midrib. Two datasets were analyzed, one from July 2015 and another from August 2015. The first dataset had 8 samples of Cabernet Sauvignon and 10 of Chardonnay, and only midrib embolisms were analyzed. In August, 14 samples of Cabernet Sauvignon and 9 of Chardonnay were obtained and their excellent resolution allowed an extensive 3D analysis of embolism in all veins of each scan and the measurement of cell dimensions to be used in our model. Each sample from August was extensively analyzed in 3D using visualization software Avizo 8.1.1 (VSG, Inc., Burlington, MA, USA). Analyses and leaf vein embolisms were quantified within the FOV in 2D and 3D using both software packages (i.e. Fiji and Avizo). The high resolution of the scans allowed us to determine whether xylem conduits were filled with water or air in each individual vein of all vein orders within the FOV. Each individual vein was examined in transverse cross-section, paradermal, and longitudinal views for the presence of embolisms.

Measuring leaf hydraulic conductance (K_{leaf})

K_{leaf} was measured using the EFM protocol (Sack *et al.*, 2002; Sack and Scoffoni, 2012; Scoffoni *et al.*, 2012) with some adaptations. The night prior to performing measurements, potted plants grown in a greenhouse were watered until the soil was saturated, and placed inside a closed dark plastic bag filled with wet paper towels to maintain high humidity and avoid transpiration. The following morning, shoots were excised under water and submerged for 30–60 s. Shoots were recut under water from the end toward the tip until only four healthy mature leaves remained, which were bench-dried to achieve a range of water potentials. Leaves were then placed in plastic bags (Whirl-Pak, Nasco) that have been previously humidified (i.e. exhaled into) and the whole shoot was then placed inside a large bag with wet paper towels to avoid transpiration. After being allowed to equilibrate for at least 30 min, the water potential of both proximal and distal leaves was measured using a digital pressure chamber (Model 1000D, PMS Instruments) and, if the difference between water potential of both leaves was >0.2 MPa (or 0.3 MPa for very dehydrated shoots), then samples were discarded. One of the two leaves in the middle of the shoot was chosen for the flow measurements. The bagged leaf still attached to the shoot was excised in the stem–petiole junction with a fresh razor blade under ultrapure degassed water in a new sterilized Petri dish. Distilled water had been degassed with a vacuum pump (Gast, Bent Harbor, MI, USA) overnight on the day preceding measurements and then refiltered (0.22 μm, Syringe Filter, EMD Millipore, Billerica, MA, USA). This water was used for cutting the leaves under water in the Petri dishes and it was supplied to the leaves during the measurements. Parafilm was then wrapped around the base of the petiole and it was recut under water, where it was immediately inserted in tubing connected to a cylinder filled with ultrapure degassed water inside a ±10 μg sensitivity analytical balance (models MS205DU and AB135-S, Mettler Toledo, Columbus, OH, USA). Flow was measured as the rate of water loss in the cylinder. The sample leaf was then placed over a fan and under a light source (500 W Halogen Work Light, Ace Hardware, Oak Brook, IL, USA) providing photosynthetically active radiation (PAR) of 1100 μmol m^{-2} s^{-1} (±200 μmol m^{-2} s^{-1}) as measured with a quantum sensor (190R, LiCor Biosciences, Lincoln, NE, USA). A water bath was placed between the leaf and the light to avoid excessive heat since leaf temperature should range between 23 °C and 28 °C to account for variations in water viscosity. The balance was connected to a data logger (CR1000, Campbell Scientific, Logan, UT, USA) and the weight of the water in the cylinder was logged every 30 s. When flow reached steady state (<5% coefficient of variation of the last 10 measurements and of the last five measurements for very low flow rates), leaf temperature was measured with a type E thermocouple placed on the abaxial side of the leaf. Steady-state flow rates had to be stable with no upwards or downwards trends, as shown in Supplementary Fig. S2, otherwise the sample was discarded. After stable steady-state flow was reached and temperature measured, the leaf was then quickly disconnected from the tubing, placed inside a humidified plastic bag, and the petiole tip was dabbed dry before placing it inside a larger bag with wet paper towels. After at least 30 min of equilibration, the final Ψ_w was measured. Leaf area was determined as the average of five measurements taken using a leaf area meter (LI-3000C and LI-3050C, LiCor Biosciences). K_{leaf} was calculated as the average of the last 10 flow rate measurements and the last five samples with very low flow divided by the most negative Ψ_w (i.e. between the average of two initials and the final), and normalized by leaf area and water viscosity at 25 °C. A vulnerability curve was generated for each cultivar, with 24 samples for Cabernet Sauvignon ranging from Ψ_{leaf}= –0.31 MPa to Ψ_{leaf}= –1.96 MPa and 23 samples for Chardonnay from Ψ_{leaf}= –0.35 MPa to Ψ_{leaf}= –2.07 MPa.

Measuring stomatal conductance

Stomatal conductance (g_s) was measured using a portable gas exchange system with a red/blue light source and a CO_2 mixing system (LI-6400XT; LiCor Biosciences). Measurements were taken in the morning between 09.00 h and 12.00 h, and in the afternoon between 15.00 h and 18.00 h in the greenhouse in 12 individuals of each cultivar. Plants were well watered on the first day of measurements and irrigation was discontinued during the experiment so plants dehydrated naturally until g_s approached zero, when the experiment was terminated. Two plants of each cultivar were kept as controls and hydrated daily until soil saturation. A young fully expanded leaf per plant was chosen on the first day and measured repeatedly throughout the experiment. Cuvette CO_2 was set at 400 ppm, PAR of 1100 μmol m^{-2} s^{-1}, similar to what was used to measure K_{leaf}, block relative humidity between 30% and 50%, and block temperature set at 25 °C. After cuvette conditions stabilized and g_s reached <1% of the coefficient of variation, data were logged five times between 30 s and 60 s, and their average was the final value. Ψ_{stem} was taken immediately after each measurement using a pressure chamber (Model 1000D, PMS Instruments) in a leaf distal to the sampled leaf and that had been previously bagged in a plastic bag lined with aluminum foil for at least 20 min prior to being measured.

Measuring turgor loss point

Pressure/volume curves were obtained from one mature leaf of five different plants of each cultivar following the protocol detailed in Sack *et al.* (2011). The 'squeeze' method was used with some modifications. Intact potted plants were rehydrated the night before measurements as for K_{leaf} measurements (see above). In the morning, a mature healthy leaf was

chosen, excised from the stem with a razor blade under water, and allowed to rehydrate for 2 min. The petiole was then carefully dried with paper tissue to avoid overestimation of water content and the leaf was equilibrated in a sealed Whirl-Pak bag previously exhaled into within a larger sealed bag with wet paper towels, and allowed to equilibrate for at least 30 min. Parafilm was wrapped around the petiole to prevent damage and prevent gas through the pressure chamber (Model 1000D, PMS Instruments) seal ring leaking during water potential measurements. The first water potential was measured and the pressure inside the chamber was held constant for 15 s after water exudation from the petiole ceased, after which the petiole tip was carefully dried with paper tissue and the pressure in the chamber was slowly released, not exceeding a rate of 0.005 MPa s^{-1}. The bagged leaf was weighed on an analytical balance (±0.1 mg; model LA230S, Sartorius, Goettingen, Germany) and then replaced in the pressure chamber. The first water potential measurement was determined as the fresh weight measurement. This procedure was repeated approximately every 0.2 MPa interval until no water was coming out of the petiole for 20 s. Finally, the leaf was placed in an oven for 48 h at 80 °C for measurement of dry weight.

Modeling the effect of anatomical changes during dehydration on water transport outside the xylem

We used a spatially explicit model of outside-xylem water transport (MOFLO 2.0; Buckley *et al.*, 2017), driven by anatomical measurements obtained from light microscopy and microCT scans, to elucidate the drivers of declining leaf hydraulic conductance during dehydration. For fully hydrated leaves, we assumed that membrane osmotic permeability to water (P_m) was equal to the default value used previously in this model (40 μm s^{-1}), whereas, for dehydrated leaves, we compared simulations with and without an 80% reduction in P_m hypothetically caused by dehydration (i.e. P_m of either 40 μm s^{-1} or 8 μm s^{-1}). For all leaves, we compared simulations with and without apoplastic water transport across the BS blocked by a hydrophobic Casparian-like barrier in the BS cell walls.

Light microscopy of cells and tissues within leaves

Measurements of cells and tissues of leaves (Supplementary Table S1) were taken from 2D leaf cross-section light microscopy images obtained following a previously used protocol (John *et al.*, 2013). Three different leaves from each cultivar were used to make the measurements. Samples were then sectioned using glass knives at 0.5 μm thickness in a rotary microtome. Sections were stained in 0.01% toluidine blue in 1% sodium borate. Images observed in the microscope (Leica M205C, Wetzlar, Germany) were acquired with a digital microscope camera (Leica DFC 425) attached to it using ×10, ×20, and ×40 magnifications, and captured with the Leica Application Suite Software (Leica Microsystems CMS GmbH). Measurements were taken from images at ×20 magnification using Fiji (FIJI-ImageJ version 1.46r; National Institutes of Health) with a 2.7767 pixel $μm^{-1}$ resolution and were obtained from three randomly chosen locations within the mesophyll in both sides of the midrib.

MicroCT scans during dehydration

Measurements were obtained from 2D cross-sectional images of slices of the same scans used for embolism quantification. Using Fiji-ImageJ across each scan analyzed, cell thicknesses of the epidermis (upper and lower), and palisade and spongy mesophylls were randomly measured in five cells from three slices (i.e. cross-sectional images) along the stack of images on both sides of the midrib (i.e. the midrib was in the center of scans as shown in Fig. 1). Leaf porosity in both palisade and spongy mesophylls was measured in five slices across the same stack of images and on both sides of the midrib.

Vein length per leaf area

Vein length per leaf area (VLA) was measured on minor veins of both cultivars from the microCT scans using the digital tracing tool in the software Dragonfly [Object Research Software (ORS) Inc., Montreal, Canada]. VLA was measured in a subregion of the scanned FOV (0.48 mm^2, ±0.04 SE, n=23), which permitted an accurate measurement of minor veins on a small region of the leaf lamina. A 3D analysis was

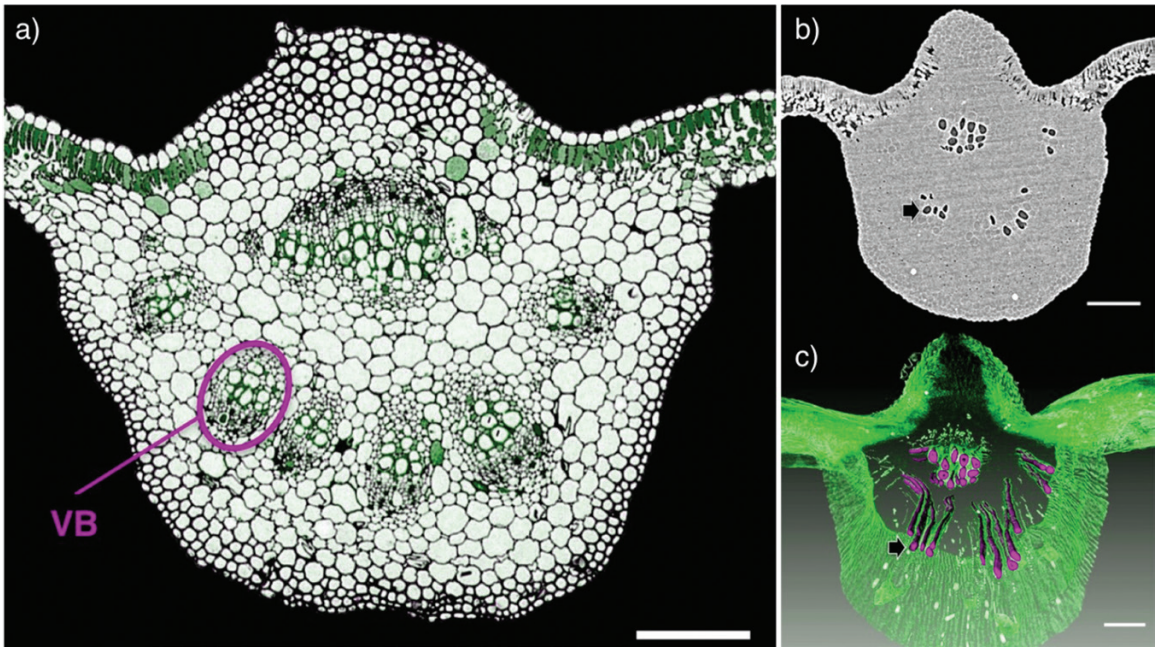

Fig. 1. Leaf midrib of *Vitis vinifera* L. cv. Cabernet Sauvignon. (A) Light microscopy showing vascular bundles (VB) and a portion of mesophyll. (B) MicroCT slice of midrib 2D cross-section with embolized conduits (darker) and a portion of the mesophyll. Note that water-filled conduits in the vascular bundle can be seen by their brighter outline. (C) 3D reconstruction of the same leaf in (B) showing how embolism was analyzed. Samples were analyzed in 3D in all planes (*x*,*y*,*z*), allowing us to fully visualize the leaf xylem network, including each vein individually and its connectedness. Only embolized conduits are represented. The arrow in (B) and (C) is pointing to the same embolized conduit. Xylem branching and embolism spread to the secondary vein can be visualized in this conduit as it bends towards the left side while others in the same vascular bundle continue in a straight direction in the midrib. Scale bar=200 μm. (This figure is available in color at *JXB* online.)

performed on the sampled region to identify all the veins as well as its connections and diameters along the axes (x,y,z) to determine vein orders. When all veins were identified, their lengths were measured using digital tracing.

Statistics

Both K_{leaf} and g_s curves were constructed after being tested for the best fit with models previously used in the literature (Scoffoni *et al.*, 2017*b*). Four functions were tested: a linear function; a three-parameter sigmoidal function; a logistic function; and an exponential function. The y in the equations represents K_{leaf} or g_s, and Ψ_w the water potential. The function choice was based on the lowest Akaike information criterion (AIC) corrected for low n and, if the difference was <2, the function with higher r^2 was selected as the maximum likelihood. Plots were constructed using SigmaPlot v.13 (Systat Software, San Jose, CA, USA). A best fit curve was generated for embolism of midrib veins for each cultivar, with 24 samples for Cabernet Sauvignon ranging from Ψ_{leaf}= –0.31 MPa to Ψ_{leaf}= –1.96 MPa and 23 samples for Chardonnay from Ψ_{leaf}= –0.35 MPa to Ψ_{leaf}= –2.07 MPa.

Results

Drought-induced embolism in grapevine leaves was primarily restricted to the midrib and occurred after the turgor loss point when K_{leaf} and g_s declined close to zero. MicroCT scans of intact leaves still attached to drying plants showed little to no embolism at tensions considered as severe water stress for wine grapes (Figs 2, 3) according to a previously established classification for field-grown *V. vinifera* (see the Materials and methods).

Both cultivars exhibited similar sigmoidal vulnerability curves, with a sharp increase in midrib embolized conduits below Ψ_w= –1.5 MPa, with 25/41 samples exhibiting midrib embolisms (Fig. 5). Cabernet Sauvignon showed slightly greater vulnerability than Chardonnay at embolism inception, having five midrib conduits embolized at Ψ_w= –1.35 MPa, while Chardonnay reached the same number at Ψ_w= –1.65 MPa. As tensions increased, both cultivars showed less difference, with Chardonnay exhibiting a steeper slope, reaching 20 midrib embolized conduits at Ψ_w= –1.91 MPa, while Cabernet Sauvignon had 20 midrib embolized conduits at Ψ_w= –2 MPa. Even though this increase occurred primarily in the midrib, in both cultivars some additional conduits embolized in the secondary veins at more negative Ψ_w; in 8/23 samples embolisms in the secondary veins were found and in all cases they were connected to embolisms in the midrib, showing clear connections between the two vein orders (Figs 1, 4). In 5/23 samples, only one secondary vein was embolized and at different water potentials (including one control), while the other three samples were severely dehydrated (Fig. 4) when embolisms appeared in this vein order. No clear pattern of which vascular bundles in the midrib would embolize first was observed; however, all embolisms found in secondary veins originated from the lateral vascular bundles of the midrib. Embolisms appeared in tertiary veins for only 4/23 samples analyzed, with only one that was not water stressed. In one sample of Cabernet Sauvignon at Ψ_w= –1.8 MPa, clear connections of embolisms were found in the three major veins (Fig. 4). Embolisms in minor veins (i.e. from the fourth to the sixth, including free-ending veins) only occurred at Ψ_w< –1.25 MPa and were rare, despite the very negative Ψ_w that some samples exhibited, ranging from –1.8 MPa to –2.8 MPa. Among these, the only sample that showed embolized conduits was at Ψ_w= –2.8 MPa, exhibiting a total of nine embolized conduits in the fourth-order vein and one isolated embolism in a sixth-order vein (Fig. 4). No embolism was observed in the fifth-order vein of any sample. Two samples exhibited one isolated embolized conduit each in the fourth-order vein, and both had Ψ_w> –1.5 MPa.

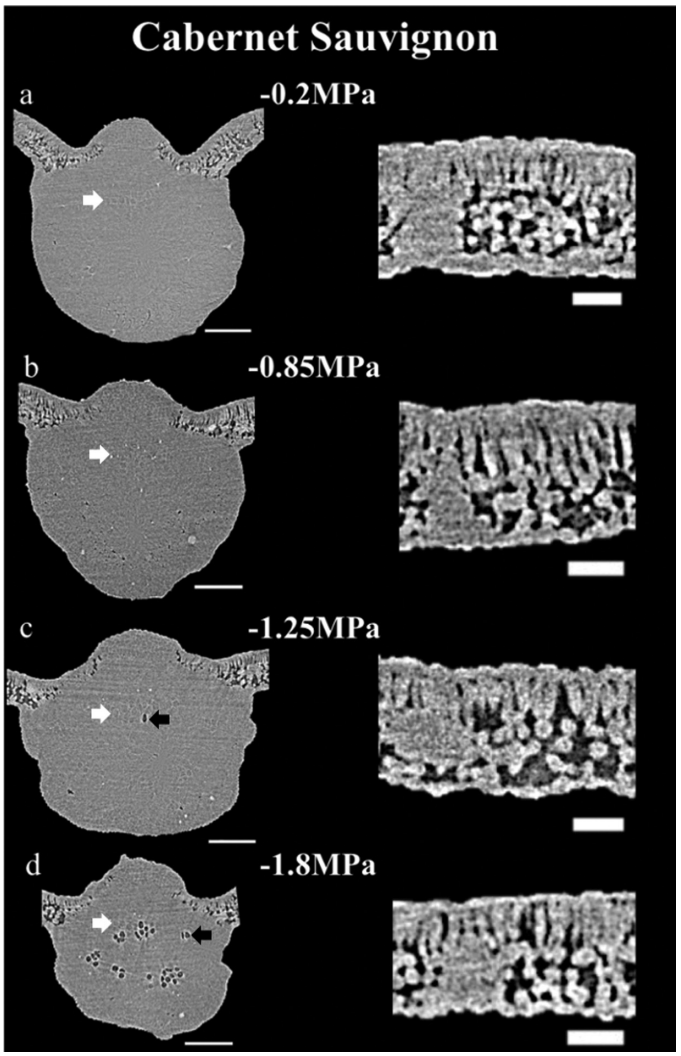

Fig. 2. Cabernet Sauvignon midrib (left column) and mesophyll (right column) microCT cross-sections of intact plants showing low vulnerability to embolism formation during drought at different stem water potentials. Each panel is a different leaf as each of them was scanned once only. Each panel show a microCT slice of a midrib cross-section with darker embolized conduits (left) and a portion of the mesophyll with a minor vein (right). Water-filled conduits can be seen by their brighter outline. (A) Control showing no embolism. (B) No embolism in the midrib but with reduced leaf thickness and cells beginning to shrink. (C) As dehydration progresses, midrib embolism initiates and mesophyll continues shrinking. (D) Midrib severely embolized, no minor vein embolism. Midrib scale=200 µm. Mesophyll scale=150 µm.

K_{leaf} appeared as very sensitive to dehydration for both cultivars, as the Ψ_w at which K_{leaf} was lost by 50% ($P_{50}K_{leaf}$) was –0.30 MPa for Cabernet Sauvignon and –0.29 MPa for

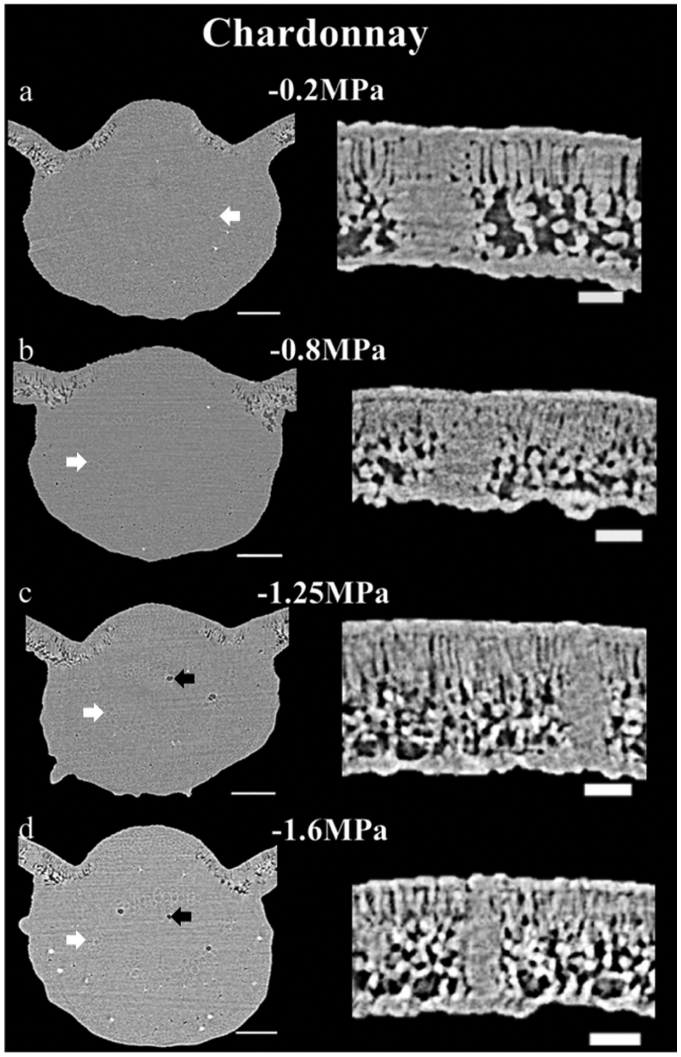

Fig. 3. Chardonnay midrib (left column) and mesophyll (right column) microCT cross-sections of intact plants showing low vulnerability to embolism formation during drought at different stem water potentials. Each panel is a different leaf as each one was scanned once only. Each panel show a microCT slice of a midrib cross-section with darker embolized conduits (left) and a portion of the mesophyll with a minor vein (right). Water-filled conduits can be seen by their brighter outline. (A) Control showing no embolism. (B) No embolism in the midrib but with reduced leaf thickness and cells beginning to shrink. (C) As dehydration progresses, midrib embolism initiates and more conduits embolize. (D) Midrib severely embolized, no minor vein embolism. Midrib scale=200 µm. Mesophyll scale=150 µm.

Chardonnay, and 80% loss of K_{leaf} ($P_{80}K_{leaf}$) occurred at Ψ_w= –0.71 MPa and Ψ_w= –0.67 MPa, respectively (Table 2; Fig. 6). These vulnerabilities of K_{leaf} to dehydration were mainly driven by the high maximum values of K_{leaf} at 0 MPa, which rarely occur in grapevines under natural conditions (Williams and Araujo, 2002; Williams and Baeza, 2007; Bota *et al.*, 2016; Charrier *et al.*, 2018). Considering Ψ_w= –0.3 MPa as the highest value, the maximum K_{leaf} is 7.32 mmol H_2O m^{-2} s^{-1} Pa^{-1} and 6.83 mmol m^{-2} s^{-1} MPa^{-1} for Cabernet Sauvignon and Chardonnay, respectively, and their vulnerabilities values change to $P_{50}K_{leaf}$ of Ψ_w= –0.61 MPa and Ψ_w= –0.56 MPa and $P_{80}K_{leaf}$ of Ψ_w= –1.02 MPa and Ψ_w= –0.95 MPa, respectively (Table 2).

Similar to K_{leaf}, g_s declined exponentially during dehydration in both cultivars (Fig. 6), with Cabernet Sauvignon exhibiting almost double the maximum g_s of Chardonnay at Ψ_w=0 MPa (0.28 mol H_2O m^{-2} s^{-1} and 0.15 mol H_2O m^{-2} s^{-1}). The cultivars showed similar decreases of g_s during dehydration, with $P_{50}g_s$ of –0.60 MPa and –0.53 MPa and $P_{80}g_s$ of –1.21 MPa and –1.17 MPa for Cabernet Sauvignon and Chardonnay, respectively. Starting the curve at Ψ_w= –0.3 MPa, the maximum values of g_s were 0.20 mol H_2O m^{-2} s^{-1} and 0.10 mol H_2O m^{-2} s^{-1} for Cabernet Sauvignon and Chardonnay, respectively, which also changed their vulnerability values. Cabernet Sauvignon thus exhibited $P_{50}g_s$= –0.85 MPa and $P_{80}g_s$= –1.37 MPa, while Chardonnay showed $P_{50}g_s$= –0.81 MPa and $P_{80}g_s$= –1.40 MPa (Table 2). K_{leaf} was more vulnerable to dehydration than g_s for both cultivars and scenarios, with the offset between $P_{50}K_{leaf}$ and $P_{50}g_s$ being ~0.25 MPa in all situations (Table 2). This difference slightly increased as Ψ_w became more negative, being ~0.4 MPa between $P_{80}K_{leaf}$ and $P_{80}g_s$. The turgor loss point (Ψ_{TLP}) was slightly less negative for Cabernet Sauvignon than for Chardonnay (Ψ_{TLP}= –1.37 MPa ±SE 0.05 and Ψ_{TLP}= –1.49 MPa ±SE 0.06, respectively).

Our model simulations showed that measured changes in leaf thickness, VLA, and porosity, the anatomical parameters that can influence MOFLO 2.0 during dehydration (Supplementary Table S2), did not explain the observed hydraulic declines in either cultivar. In fact, Cabernet Sauvignon and Chardonnay exhibited contrasting responses to our model simulations; however, the response to these anatomical changes in both cultivars was only slight. K_{ox} would increase in Cabernet Sauvignon and slightly decrease in Chardonnay during dehydration, mainly driven by changes in VLA, which increased in the former and decreased in the latter. Even with the simulated reduction in K_{ox} for Chardonnay, anatomical changes were not enough to account for the observed hydraulic decline. We found that, in order to explain the observed declines in K_{leaf} of both cultivars, it was necessary to assume an 80% reduction in membrane permeability combined with a Casparian-like band in the BS cell walls (Fig. 7, bottom panel).

Discussion

We present direct evidence that xylem embolism formation is not responsible for the coordinated decline in K_{leaf} and g_s in grapevines during drought. Neither Cabernet Sauvignon nor Chardonnay exhibited drought-induced embolism before substantial loss of K_{leaf} and g_s occurred, pointing to the outside-xylem as being mainly responsible for increased hydraulic resistance and stomatal closure during leaf dehydration. Moreover, drought-induced leaf vein embolism initiated below Ψ_{TLP}, indicating that the turgor loss was also not affected by embolism formation. We also identified patterns of embolism spread in the highly connected leaf xylem network of grapevines, while our model simulations of the outside-xylem pathways indicated that membrane permeability of the BS combined with the presence of an apoplastic barrier would account for the observed hydraulic decline during dehydration.

This is the first study combining both direct embolism observation and leaf hydraulics during dehydration in grapevines,

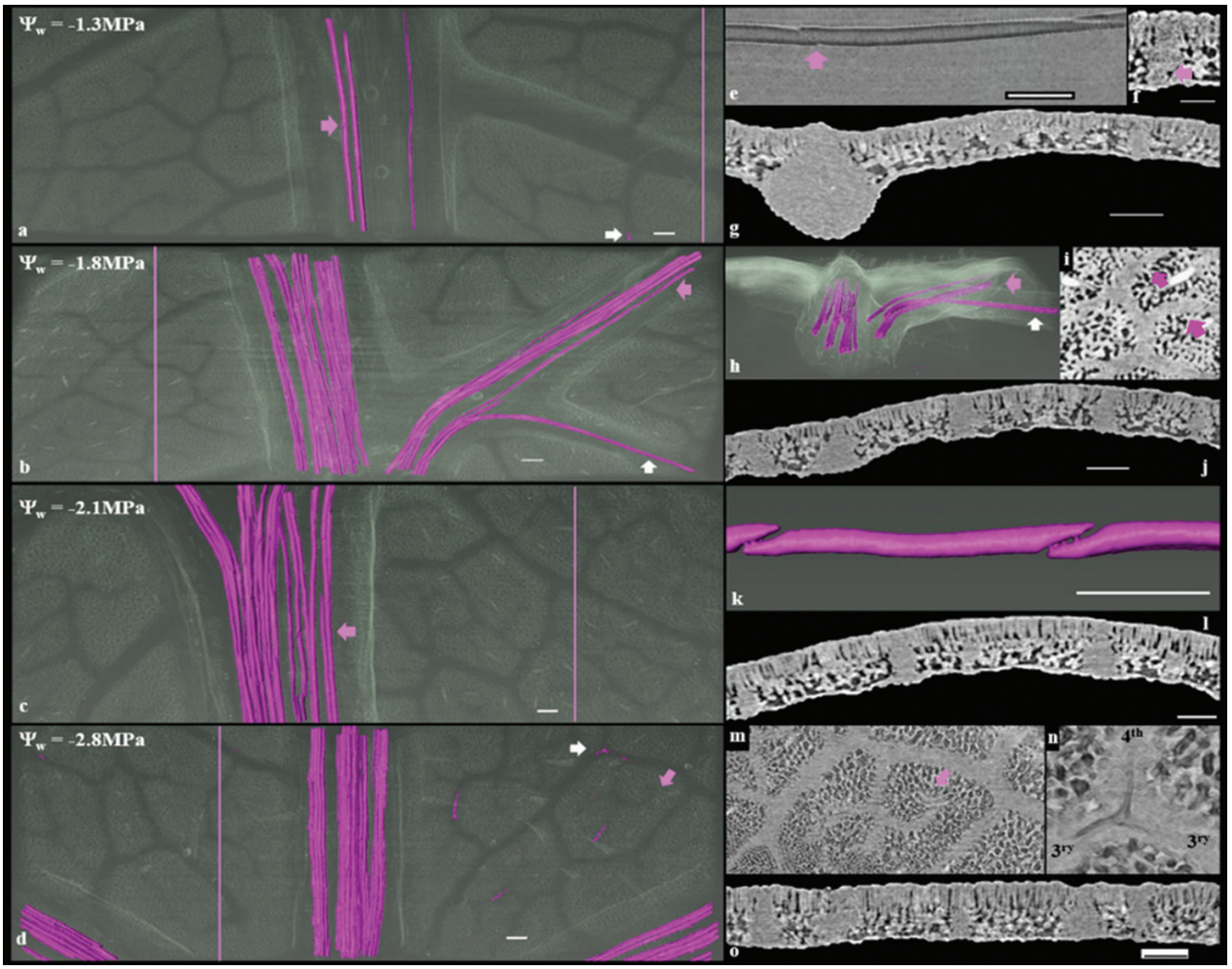

Fig. 4. Embolism during severe dehydration in leaves of *Vitis vinifera* cv. Cabernet Sauvignon. Paradermal view of 3D reconstructed grapevine leaves showing embolized xylem conduits and leaf venation (A–D). First embolisms begin to occur from around –1.3 MPa and become more common as water potential becomes more negative. Embolism occurs first in the midrib and then spreads to higher order veins through xylem branching, showing a high degree of connectivity between vessels. Water-filled xylem conduits are not shown. Panels (E–G) are from the same sample shown in (A). (E) Embolized conduit in the midrib with intervessel pit in detail as shown in (A) (arrow). (F) Isolated embolized conduit in a minor vein (fourth order) shown by the arrow, same as seen in (A). Scale bar=50 μm. Embolized conduits are dark, while water-filled are lighter and not always visible. (G) Longitudinal view of the section represented by the line in (A) showing lack of embolisms in different vein orders with a cross-section of a tertiary vein seen in detail (bright arrow). Panels (H–J) are from the same sample shown in (B). (H) 3D cross-section showing embolism spreading from the midrib to a secondary (darker arrow) and tertiary (brighter arrow) vein via xylem connectivity. (I) Free-ending veins (darker arrow) embedded in the mesophyll. (J) Longitudinal view of the section represented by the transverse line in (B), showing lack of embolisms in different vein orders. Panels (K–L) are from the same sample shown in (C). (K) Detail of a vessel element indicated by the darker arrow in (C). Scale bar=1 μm. (L) Longitudinal view of the section represented by the line in (C), showing lack of embolisms in different vein orders. Panels (M–O) are from the same sample shown in (D). (M) Free-ending veins inside the same areole of (D), indicated by darker arrows. (N) Detail of isolated embolism in tertiary and fourth-order veins indicated by the bright arrow in (D). The full embolism extent was comprised within the area shown. (O) Longitudinal view of the section represented by the line in (D), showing lack of embolisms in different vein orders. Scale bars=100 μm, except for (F) and (K). (This figure is available in color at *JXB* online.)

showing that their leaf xylem network is extremely resistant to drought-induced embolism in intact grapevine leaves of two different cultivars. Despite the importance of xylem integrity for hydraulic function and its impact on gas exchange and crop performance, so far the only study combining hydraulics and direct embolism observation was conducted on wheat by Corso *et al.* (2020) (Table 1). Xylem embolism has been commonly assigned as an important early response to dehydration in grapevines and is responsible for triggering stomatal closure (Zufferey *et al.*, 2011; Jacobsen and Pratt, 2012). However, recent studies also noted the outside-xylem water pathways as the drivers of K_{leaf} decline during drought rather than leaf xylem embolism in several species (Bouche *et al.*, 2016; Trifilò *et al.*, 2016; Scoffoni *et al.*, 2017*b*, 2018; Corso *et al.*, 2020). The idea that *V. vinifera* stems and petioles are highly susceptible to embolism and the cause for stomatal closure in wine grape cultivars (Zufferey *et al.*, 2011; Jacobsen and Pratt, 2012) has been challenged by other studies showing that they are not as vulnerable to dehydration-induced embolism in both organs (Choat *et al.*, 2010; Brodersen *et al.*, 2013; Hochberg *et al.*, 2015b) as well as leaf laminas (Hochberg *et al.*, 2017*a*). Petiole embolisms only occurred at tensions rarely experienced under field conditions and are more vulnerable to embolism events than stems, with embolism appearing in petioles

Table 1. Meta-data of studies on crop species showing water potentials at which embolisms were initially observed during dehydration and K_{leaf} vulnerabilities to drought

Authors	Species	Ψ_w of initial leaf xylem embolism observation (MPa)	K_{leaf}	
			$P_{50}K_{leaf}$	$P_{80}K_{leaf}$
This study	*V. vinifera* cv. Cabernet Sauvignon	–1.3	–0.3	–0.71
	V. vinifera cv. Chardonnay	–1.2	–0.29	–0.67
Hochberg *et al.* (2019)	*V. vinifera* cv. Chardonnay	–0.45 >Ψ_w> –1.4[a]	–	–
Hochberg *et al.* (2017*a*)	*V. vinifera* cv. Chardonnay	< –1.4	–	–
Hochberg *et al.* (2017*b*)	*V. vinifera* cv. Merlot	–0.5>Ψ_w> –0.7	–	–
Martorell *et al.* (2015)	*V. vinifera* cv. Grenache	–	–1.51>Ψ_w>–2.15	–1.81>Ψ_w> –2.59
	V. vinifera cv. Tempranillo	–	–1.58>Ψ_w> –2.22	–1.87>Ψ_w> –3.07
Trifilò *et al*. (2016)	*Vitis labrusca*	–	–1.23*	–2.07[a]
Corso *et al.* (2020)	*Triticum aestivum*	–1.5>Ψ_w> –1.8[a]	–0.91	–1.7[c]
Cardoso *et al.* (2020)	*Persea americana*	–0.9>Ψ_w > –2.32	–	–
Wang *et al.* (2018)	*Oryza sativa*	–	–0.78*	–1.43[a]
Skelton *et al.* (2017)	*Solanum lycopersicum*	–1.24	–1.54	–1.8[b]
Hernandez-Santana *et al.* (2016)	*Olea europea* cv. Arbequina	–	–1.52	–5.35
	Prunus dulcis cv. Guara	–	–1.45	–4.21
Scoffoni *et al.* (2011)	*Helianthus annuus*	–	–0.83	–1.16

[a] Data obtained from different methods and averaged K_{leaf} vulnerabilities.
[b] Indicates $P_{88}K_{leaf}$.
[c] Indicates $P_{90}K_{leaf}$.

Table 2. Values of maximum K_{leaf} and g_s for the less negative water potential considered in the vulnerabilities curves ($\Psi_{highest}$), at either 0 MPa or –0.3 MPa

Vitis vinifera cvs	$\Psi_{highest}$ (MPa)	K_{leaf}			g_s			Ψ_{TLP}
		K_{leaf} maximum	$P_{50}K_{leaf}$	$P_{80}K_{leaf}$	g_s maximum	$P_{50}g_s$	$P_{80}g_s$	
		(mmol H_2O m^{-2} s^{-1} MPa^{-1})	(MPa)	(MPa)	(mol H_2O m^{-2} s^{-1})	(MPa)	(MPa)	(MPa)
Cabernet Sauvignon	**0**	14.52	–0.30	–0.71	0.279	–0.60	–1.21	–1.37±0.05
	–0.3	7.32	–0.61	–1.02	0.199	–0.85	–1.37	
Chardonnay	**0**	13.90	–0.29	–0.67	0.153	–0.53	–1.17	-1.49±0.06
	–0.3	6.83	–0.56	–0.95	0.104	–0.81	–1.40	

Water potentials at which K_{leaf} and g_s declined by 50% (P_{50}) and 80% (P_{80}) varied depending on the $\Psi_{highest}$. Turgor loss points (Ψ_{TLP}) with SE (n=5) are shown in the last column

at a Ψ_w of approximately –1.1 MPa (Hochberg *et al.*, 2015a). Recent findings with the same cultivars as we investigated herein showed that the inflection point for loss of hydraulic conductivity in petioles of Cabernet Sauvignon was around Ψ_w= –1.0 MPa (Hochberg *et al.*, 2015b) while embolism inception in Chardonnay leaves occurred at a Ψ_w of approximately –1.4 MPa and after stomatal closure (Hochberg *et al.*, 2017*a*). Our results are in good agreement with those studies in both embolism thresholds and shape of the curves; as xylem conduits of grapevine petioles extend to the midrib (Chatelet *et al.*, 2006; Thorne *et al.*, 2006), it is expected that petioles and midribs would exhibit similar vulnerabilities to embolism. The mild discrepancies in embolism thresholds between studies may be due to differences in growing conditons and/or plant size. Moreover, we found in both cultivars that embolism initiated after stomatal closure.

Both Chardonnay and Cabernet Sauvignon showed similar vulnerability to embolism, where the larger xylem conduits of the leaf midrib were the first ones to embolize, most probably due to the fact that they have the larger diameters of the leaf xylem network (Scoffoni *et al.*, 2017*a*). As the conduits in the midrib are the main suppliers of water coming from the petioles, embolized conduits in the midrib could have a strong impact on whole-leaf hydraulic supply. Despite the fact that midrib embolism inception in Cabernet Sauvignon occurred slightly earlier than in Chardonnay, the very few embolized conduits would not account for the observed decline in both K_{leaf} and g_s due to the redundancy of midrib xylem conduits and the water potential values at which it happened. Midrib embolism initiated when K_{leaf} was reduced by 94% in Cabernet Sauvignon and 96% in Chardonnay, which is strong evidence that the outside-xylem pathways are responsible for the hydraulic impairment of grapevine leaves during drought, and not xylem embolism. As leaves experience the most negative tensions in the soil–plant–atmosphere continuum, in the light of the hydraulic segmentation hypothesis (Tyree and Ewers, 1991), the living cells of the outside-xylem would be the first and main circuit breaker of the plant water transport system,

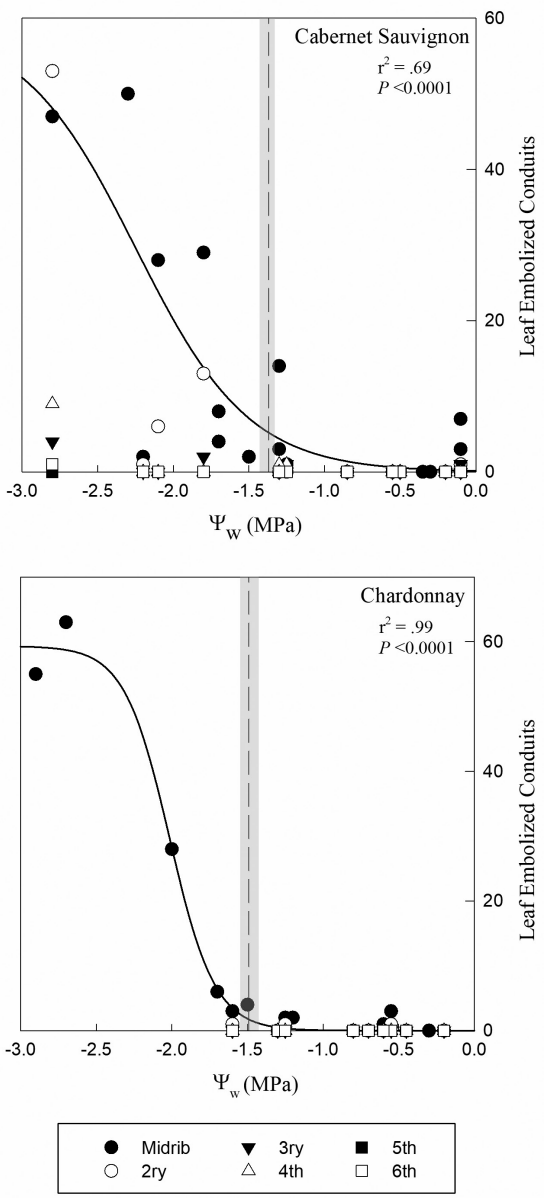

Fig. 5. Number of embolized xylem conduits per vein order in intact leaves of grapevine during drought, showing that embolisms initiated in the midrib and spread to higher order veins with increasing tensions in the xylem. Analyses were performed in full 3D reconstructions, so all veins could be individually analyzed. (A) Cabernet Sauvignon showing initiation of xylem embolism around Ψ_{leaf}= −1.3 MPa in the midrib with embolisms spreading to the secondary vein at higher tensions. Few embolisms were observed in higher order veins and only at very negative water potential values. Only one embolized conduit was found in a sixth-order vein (i.e. free-ending vein) and in the most water-stressed sample (Ψ_{leaf}= −2.8 MPa). (B) Chardonnay leaves showed slightly less initial vulnerability to drought-induced xylem embolism formation than Cabernet Sauvignon, with midrib embolism inception at more negative water potentials. Midrib embolism greatly increased for both cultivars when Ψ_{leaf} was ≤ −1.5 MPa with a steeper slope for Chardonnay. The most stressed Chardonnay sample with resolution to resolve for minor vein embolisms was at Ψ_{leaf}= −1.6 MPa. Best fitted curves are only for midrib embolisms and were three-parameter sigmoidal. For Cabernet Sauvignon $y=59.2179/<1+e^{\{-[\Psi w-(2.2492)]/(-0.3760)\}}>$ and for Chardonnay $y=59.3279/<1+e^{\{-[\Psi w-(2.0151)]/(-0.1496)\}}>$. Statistical data are shown in each panel. For embolism analysis in midribs, n=41. A subset of n=23 was analyzed for embolisms in all vein orders within each scan (see the Materials and Methods for further details). The dashed vertical line represents Ψ_{TLP} and the gray shadowed area the SE. First embolisms occurred only at around or past Ψ_{TLP}.

acting to prevent increased tensions that could induce embolism in the leaf xylem. This would be especially important in grapevines due to their wide and large xylem conduits spanning from leaves to stems (Choat *et al.*, 2010).

These findings indicate that the leaf xylem network of grapevine leaves is very resistant to drought-induced embolism formation despite its high degree of connectivity and the most negative tensions in the xylem being experienced by the minor veins. As water potentials became more negative after stomatal closure, loss of K_{leaf}, and inception of embolism in midribs of both cultivars, embolism spread mainly to secondary and a few tertiary veins. This clear pattern of embolism spread with further dehydration was observed in all samples that showed embolism in secondary veins, since all conduits observed in secondary veins were branching from the lateral vascular bundles of the midrib and in one sample an embolism from the midrib spread to a tertiary vein. Even though there was no clear pattern of which midrib vascular bundles are the first to embolize, embolism spread seems to occur downstream of the water potential gradient and towards leaf margins, as embolisms that did not branch to secondary veins continued in the midrib towards the leaf tip. These findings are in good agreement with those reported by Thorne *et al.* (2006) in two grapevine species, showing that air can move from the midrib up to tertiary veins and towards the leaf margins via open conduits. In a follow-up study, Chatelet *et al.* (2006) attributed the lack of air movement to minor veins to xylem anatomy, as tracheids would replace vessels below this vein order, thus explaining why air never reached leaf margins in both the aforementioned studies. We can thus infer that leaf margins are the most stressed part of the leaves and exposed to the greatest water potential gradients, therefore generating higher tensions downstream of the xylem network. Corroborating these ideas, the few isolated embolized conduits we observed in higher order veins (Figs 4, 5) were only found at very negative Ψ_w values that are not experienced by plants in vineyards (Choat *et al.*, 2010; Charrier *et al.*, 2018). The lack of embolism in minor vein conduits can also be explained by their narrow diameters, which would require extremely high tensions to induce embolism, as predicted by the rare-pit hypothesis (Christman *et al.*, 2009, 2012) and/or by having short conduits as well as more resistant pit membranes. Indeed, a recent study in dehydrating leaves of several species also showed few and isolated embolisms in minor veins (Scoffoni *et al.*, 2017*a*). In Arabidopsis, simulations of hydraulic dysfunction of higher order veins by collapse would have a minor impact in K_{leaf} and even in K_x decline during dehydration (Scoffoni *et al.*, 2018). Contrary to Zhang *et al.* (2016), we found no evidence of collapse of leaf minor vein conduits even at extreme dehydration.

The similar vulnerabilities that both cultivars exhibited in K_{leaf} and g_s aligned with the absence of xylem embolism indicate a tight regulation of K_{leaf} by the outside-xylem pathways and its close coordination with g_s during dehydration. Both Chardonnay and Cabernet Sauvignon showed similar K_{leaf} vulnerabilities to drought as well as K_{max} values, exhibiting a very sensitive response to early dehydration. We then tested how these vulnerabilities would change assuming $\Psi_{highest}$= −0.3 MPa, since plants rarely experience smaller tensions in vineyards and those were the greatest water potentials in our

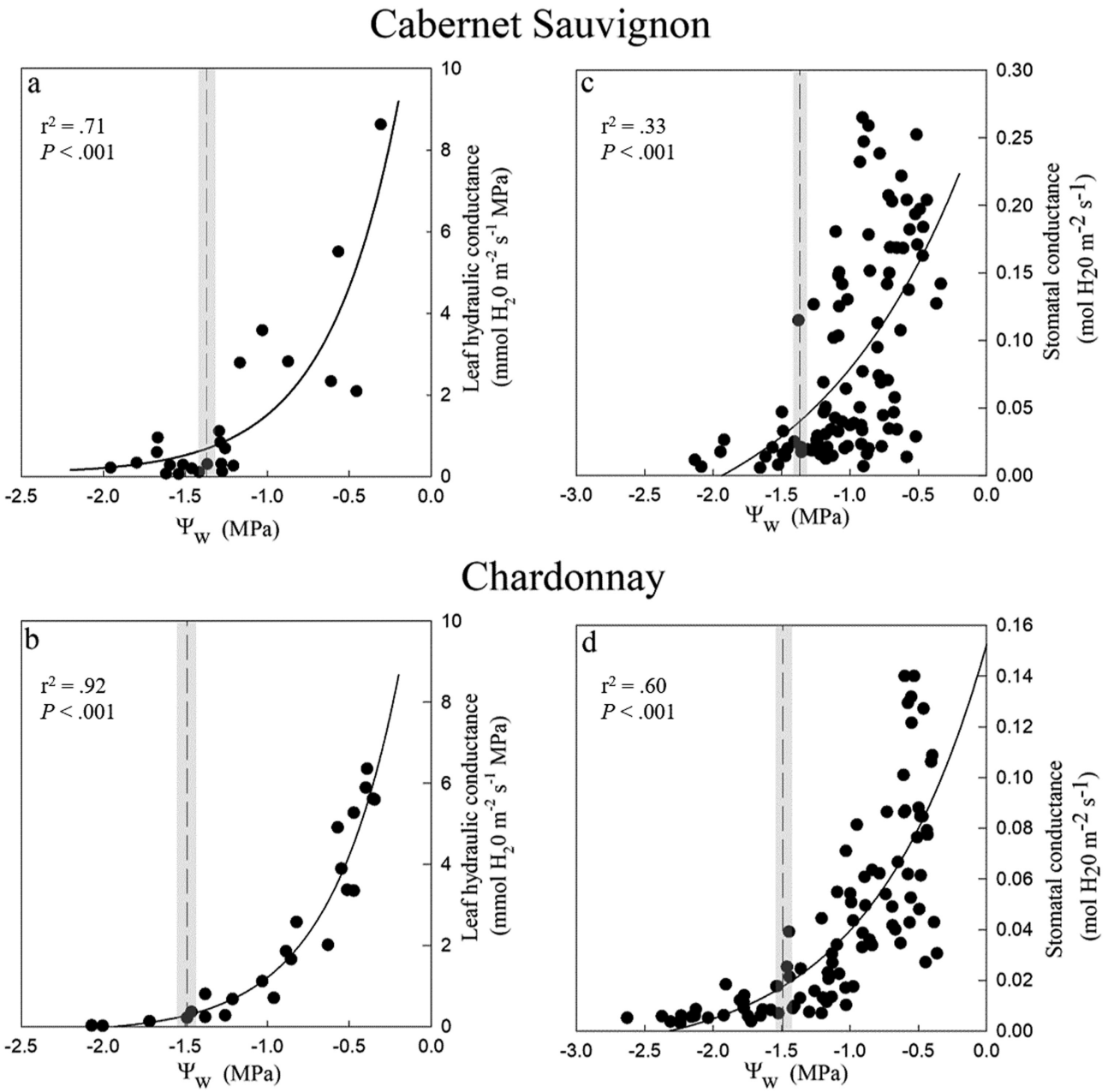

Fig. 6. Leaf hydraulic conductance (K_{leaf}) and stomatal conductance (g_s) of Cabernet Sauvignon (A–C) and Chardonnay (B–D) during dehydration. Cabernet Sauvignon exhibited greater vulnerability to dehydration; however, both cultivars reached P_{80} before the initiation of embolism events. Both cultivars showed similar K_{leaf} values along the dehydration range (A, B). Cabernet Sauvignon showed absolute g_s values around twice as high as Chardonnay along the curve, indicating that even at the same water stress level it has twice the amount of gas exchange as Chardonnay. Best fitted curves were three-parameter exponential: y=0.071 + 14.453e$^{-(-2.302)\Psi w}$, n=24 (A); y= –0.155 + 14.060e$^{-(-2.331)\Psi w}$, n=23 (B); y= –0.061 + 0.334e$^{-(-0.884)\Psi w}$, n=102 (C), and y= –0.011 + 0.1634e$^{-(-1.180)\Psi w}$, n=94 (D). Statistical data are shown in each panel. The dashed vertical line represents Ψ_{TLP} and the gray shadowed area the SE.

gas exchange measurements. These simulations did not affect our findings, as xylem embolism occurred after K_{leaf} was almost zero and the turgor loss point has been reached in both cultivars, with $P_{50}K_{leaf}$ and $P_{80}K_{leaf}$ ~0.3 MPa more negative, reflecting changes in K_{max}. These results highlight the importance of including very high water potentials near full hydration (i.e. close to Ψ_w=0 MPa) in vulnerability curves for a more uniform and better understanding of how susceptible species are to dehydration, as proposed in the Ferrari argument by Scoffoni and Sack (2017). Recently, a modeling study proposed that the loss of soil hydraulic conductivity is the driver of stomatal closure in medium-wet to dry soils (Carminati and Javaux, 2020); however, K_{leaf} was not accounted for in their model and the outside-xylem pathways were not considered. Our findings in grapevines show that the complex water transport pathways in living cells of the outside-xylem are responsible for the coordinated K_{leaf} and g_s decline. Moreover, stomata are in the leaves and exposed to atmospheric vapor pressure deficit (VPD), so they may close even if exposed to high VPD despite a wet soil. As g_s decline was less sensitive than

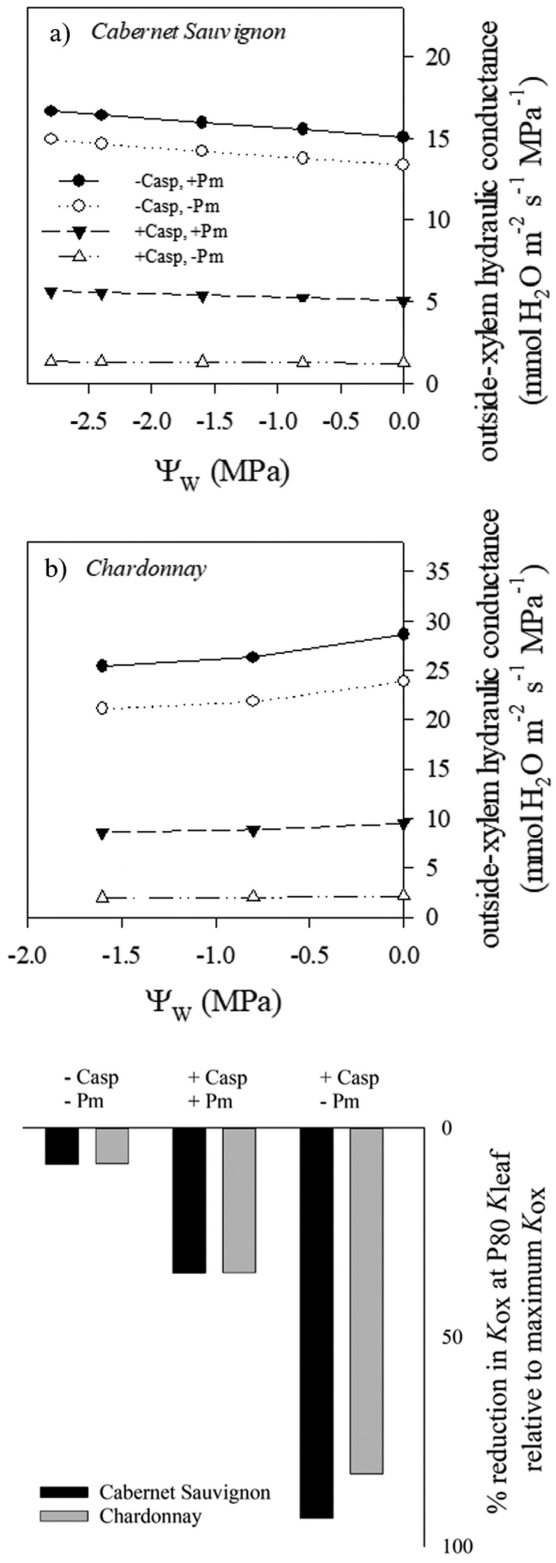

Fig. 7. The model MOFLO 2.0 was used to simulate the anatomical effects of dehydration on the outside-xylem hydraulic conductance (K_{ox}). Cabernet Sauvignon (A) showed a slight increase in K_{ox} during dehydration while Chardonnay (B) exhibited a slight reduction in K_{ox} with dehydration. The anatomical changes were mainly driven by leaf shrinkage and did not explain the observed leaf hydraulic declines for either cultivar shown previously. However, if membrane permeability, P_m, is assumed to decline by 80% ('–P_m') at low water potential, and if all water transport across the bundle sheath is assumed to be forced across membranes by a hydrophobic cell wall barrier (Casparian strip; '+Casp'), then K_{ox} is predicted to decline as observed experimentally (bottom plot). As xylem embolism only occurred after K_{leaf} was lost and K_{leaf} is composed of both K_x and K_{ox}, and the model is for K_{ox} only, we assume that K_{leaf} is the same as K_{ox}.

K_{leaf} during dehydration, other factors may also be playing a role in the slower g_s decline such as water stored in the leaf as well as reduced soil and roots hydraulic conductivity. Indeed, a study in grapevine roots showed that cortical lacunae formation reduced root hydraulic conductivity before root shrinkage and xylem embolism during dehydration (Cuneo *et al.*, 2016). Integrated studies that combine both leaf and root responses to dehydration taking into account their living tissues will be crucial for a more comprehensive understanding of mechanisms involved in whole-plant responses to drought that does not take the xylem as the sole plant water transport pathway.

Stomatal conductance of both cultivars exhibited similar vulnerabilities to dehydration and little to no influence of xylem embolism; however, cultivars differed in their maximum and thus absolute values of g_s along the curves. On average, g_s of Cabernet Sauvignon was double that of Chardonnay, and this difference increased as Ψ_w became more negative. Maximum values of g_s were twice as large for Cabernet Sauvignon as for Chardonnay in either Ψ_{max} scenario tested (Table 2) and, as curves for both cultivars behaved similarly, this trend continued along the dehydration range. The offsets of $P_{50}g_s$ and $P_{80}g_s$ between scenarios were ~0.2 MPa in both cultivars, similar to what was found for K_{leaf}. Even in the $\Psi_{highest}$= –0.3 scenario when $P_{80}g_s$ was at Ψ_w= –1.4 MPa for both cultivars, still the few midrib embolisms found at this range would most probably not account for the observed declines in g_s as leaf vein redundancy would buffer the few embolized conduits from affecting xylem hydraulic transport. Contrasting with our findings, Zufferey *et al.* (2011) reported that daily fluctuations in g_s in a wine grape cultivar were due to petiole embolism formation and repair. Even though grapevines have the ability to repair embolisms to restore xylem hydraulic function (Holbrook *et al.*, 2001; Knipfer *et al.*, 2016), this requires that water potentials approach 0 MPa, which rarely occurs under field conditions especially for deficit-irrigated plants. Zufferey *et al.* (2011) also reported 90% loss of conductivity due to petiole embolisms by –1.3 MPa when using hydraulics on excised samples, while we found in intact plants that embolisms begin to appear in leaf midribs at a Ψ_w of approximately –1.25 MPa. Another study in grapevine leaves showed that embolism only occurred after complete stomatal closure (Hochberg *et al.*, 2017*a*), even though their results might have been affected by the low light intensity used in their experiments.

The very close coordination that both cultivars showed between K_{leaf} and g_s during dehydration indicates an intermediate behavior between anisohydric and isohydric that lead us to further reject those categories for the wine grape cultivars of this study. Much attention was given to classifying wine grape cultivars as one or other of these categories since Schultz (2003); however, a recent study with several field-grown wine grape cultivars showed that they exhibit a continuum of stomatal responses during drought and challenged the exclusive classification of wine grapes as either isohydric or anisohydric (Levin *et al.*, 2019). Our findings that K_{leaf} strongly regulates g_s agrees with our previous study in Arabidopsis (Scoffoni *et al.*, 2018), while a more recent study concluded that K_{leaf} was not the direct driver of g_s decline during dehydration in wheat (Corso *et al.*, 2020). However, Schultz (2003) also observed a strong correlation between g_s and estimated K_{leaf} in two field-grown wine grape cultivars despite their different hydraulic

responses to drought. The close matching between K_{leaf} and g_s decline during dehydration is of great advantage for crop species, especially grapevines that not only are commonly grown under hot and dry conditions but that also benefit from water deficits, differently from annual crop species. This intermediate behavior brings benefits from both isohydric behavior by maintaining leaf tissues hydration and anisohydric behavior by avoiding embolism formation and keeping gas exchange during dehydration (Scoffoni and Sack, 2017). While the former may contribute to a fast recovery of gas exchange upon rehydration (i.e. irrigation), the latter allows stomata to remain open, thus ensuring carbon capture during further dehydration while also protecting the hydraulic system from embolism events, especially if K_{leaf} increased resistance is driven by the outside-xylem (Scoffoni and Sack, 2017). Interestingly, we observed that despite the close matching between K_{leaf} and g_s, with K_{leaf} being slightly more vulnerable to dehydration in all cases (Table 2), this small difference of ~0.26 MPa at P_{50} vulnerabilities changed to ~0.45 MPa when P_{80} values were compared. Even if small, this indicates that as dehydration increases wine grapes may exhibit a near-anisohydric behavior, which agrees with recent findings that wine grape cultivars may exhibit different behaviors depending on the degree of dehydration (Levin *et al.*, 2019) and that stomata remain open until the brink of embolism events in the midrib. This larger difference in vulnerabilities between K_{leaf} and g_s as dehydration becomes more severe would reduce leaf water supply more rapidly than it is lost, thus decreasing Ψ_w and turgor, which would further contribute to amplify stomatal closure. Grapevines would then avoid embolism formation that may compromise long-term hydraulic function while also ensuring carbon capture at higher tensions. Even though cultivars had similar responses to dehydration, the slightly lower vulnerability that Cabernet Sauvignon exhibited in comparison with Chardonnay aligned with the higher g_s values measured in the former, indicating that Cabernet Sauvignon may lose more water under well-watered conditions than Chardonnay. However, it may be an advantage in terms of energy balance in hotter conditions where Cabernet Sauvignon is preferentially grown, while Chardonnay is more commonly cultivated in cooler regions. Interestingly, both showed similar Ψ_{TLP}, with Chardonnay being slightly more negative, and even this small difference is contrary to what would be expected.

The absence of leaf xylem embolisms indicates that the living tissues of the outside-xylem are the down-regulators of K_{leaf} and thus of g_s decline during mild dehydration in grapevine leaves. Our modeling results indicated that only an 80% reduction in membrane water permeability (perhaps through reduced aquaporin expression or activity) combined with the presence of a Casparian-like band in the BSs would account for the decline in K_{leaf} during drought for both Cabernet Sauvignon and Chardonnay. Indeed, deactivation of aquaporin expression has been attributed to reducing K_{leaf} during drought (Kim and Steudle, 2007; Shatil-Cohen *et al.*, 2011; Pantin *et al.*, 2013; Pou *et al.*, 2013; Sade *et al.*, 2014, 2015). In grapevines, a study with two wine grape cultivars including Chardonnay showed reduced aquaporin expression in leaves and petioles in response to dehydration (Shelden *et al.*, 2017), and another showed that the expression of several aquaporin genes is down-regulated at moderate water stress and more strongly in leaves than in roots (Galmés *et al.*, 2007). This tight control would not only avoid excessive water loss and prevent xylem embolism formation, but would also allow rapid recovery of g_s, since it is more likely to occur if it depends on recovery of cell turgor and/or aquaporin activation (Martre *et al.*, 2002; Cochard *et al.*, 2007; Pou *et al.*, 2013; Sade *et al.*, 2015). As water leaves the xylem and crosses the parenchyma cells, it flows through the BS before entering the mesophyll. The presence of a suberized or lignified Casparian-like hydrophobic band in the BS would force the water to flow across the living cells (i.e. via the symplast or transmembrane) since the suberized cell walls would greatly reduce water flow through the apoplast (i.e. porous cell walls), similarly to roots. These apoplastic barriers have been shown in leaves of some species (Lersten, 1997; Mertz and Brutnell, 2014; Taneda *et al.*, 2016). In grapevines, suberin accumulation in response to water stress was seen in roots (Vandeleur *et al.*, 2009) and around vascular bundles in petioles (Hochberg *et al.*, 2013). If existent, then water would preferentially flow across the BS cells and aquaporins would have a major role in leaf hydraulic conductance. As leaf dehydration progresses, aquaporin activity would be reduced and water flow greatly diminished. Water then would encounter great resistances to flow across cells without these water-specific membrane-bound channels and through the hydrophobic suberized Casparian-like band in the apoplast. Aquaporin deactivation was also attributed to stomatal closure in grapevines (Pou *et al.*, 2013), and modeling results from recent studies indicate that the membrane permeability due to aquaporin activity would be the cause of the observed K_{leaf} decline during drought in five angiosperm species from different ecological habitats (Scoffoni *et al.*, 2017*b*, 2018).

In conclusion, our results reveal that the tensions required to induce embolism are rarely experienced in commercial vineyards. Additionally, we report that embolism formation in minor veins is negligible, only rarely occurring at Ψ_w values that are extremely negative and the plant is most probably near death. The finding that grapevines are highly resistant to drought-induced embolism formation may help explain why grapevines thrive in hot and dry regions and water deficit is a widely utilized tool to grow grapes. Furthermore, upon rehydration, grapevines could rapidly recover hydraulic function, thus ensuring carbon gain. Finally, even though both cultivars studied showed similar vulnerabilities to drought-induced leaf embolism formation, leaf hydraulics, and K_{leaf}, they also exhibited very different values of g_s. Therefore, their apparent different responses to drought could come from having different gas exchange values despite having very similar vulnerabilities. Future work should address the hydraulic role of living tissues of the outside-xylem in grapevine leaves as well as molecular components in them during drought.

Supplementary data

The following supplementary data are available at *JXB* online.

Table S1. Leaf anatomical parameters measured from light microscopy of Cabernet Sauvignon and Chardonnay used in MOFLO 2.0.

Table S2. Leaf anatomical parameters measured from microCT scans of intact leaves of Cabernet Sauvignon and

Chardonnay across a dehydration range used in MOFLO 2.0.

Fig. S1. Location on the leaf where scans were targeted and paradermal view of midrib and leaf venation embed in the mesophyll.

Fig. S2. Raw flow data of leaf hydraulic conductance of Cabernet Sauvignon and Chardonnay using the Evaporative Flux Method (EFM).

Acknowledgements

We thank Dula Parkinson and Alastair McDowell for technical assistance, and the Advanced Light Source in Berkeley, California (Beamline 8.3.2) and the Foundation Plant Services (FPS) at Davis for donating plant material. This work was supported by the USDA-ARS Sustainable Vineyard Production Systems CRIS (2032-21220-006-00-D) and CAPES/Brazil. The Advanced Light Source is supported by the Director, Office of Science, Office of Basic Energy Sciences, of the US Department of Energy under contract no. DE-AC02-05CH11231. We also thank Thorsten Knipfer, Italo Cuneo, Clarissa Reyes, and Daniel Ribeiro for technical assistance. CA was supported by a CAPES/Brazil PhD Scholarship. CS and LS were supported by the US National Science Foundation (award #1457279). TNB was supported by the National Science Foundation (award #1557906) the USDA National Institute of Food and Agriculture (Hatch project 1016439) and the Almond Board of California (18.HORT37).

Author contributions

CA and AJM conceived the study and designed the experiments. CA performed the experiments and analysed the data. TNB ran the modeling. CA and AJM wrote the manuscript with input from all authors.

Data availability

The data supporting the findings of this study are available from the corresponding author, Andrew McElrone, upon request.

References

Bota J, Tomás M, Flexas J, Medrano H, Escalona JM. 2016. Differences among grapevine cultivars in their stomatal behavior and water use efficiency under progressive water stress. Agricultural Water Management **164**, 91–99.

Bouche PS, Delzon S, Choat B, Badel E, Brodribb TJ, Burlett R, Cochard H. 2016. Are needles of *Pinus pinaster* more vulnerable to xylem embolism than branches? New insights from x-ray computed tomography. Plant, Cell & Environment **39**, 860–870.

Brodersen CR, McElrone AJ, Choat B, Lee EF, Shackel KA, Matthews MA. 2013. In vivo visualizations of drought-induced embolism spread in *Vitis vinifera*. Plant Physiology **161**, 1820–1829.

Brodribb TJ, Holbrook NM. 2004. Diurnal depression of leaf hydraulic conductance in a tropical tree species. Plant, Cell & Environment **27**, 820–827.

Bucci SJ, Scholz FG, Goldstein G, Meinzer FC, Sternberg LDSL. 2003. Dynamic changes in hydraulic conductivity in petioles of two savanna tree species: factors and mechanisms contributing to the refilling of embolized vessels. Plant, Cell & Environment **26**, 1633–1645.

Buckley TN, John GP, Scoffoni C, Sack L. 2017. The sites of evaporation within leaves. Plant Physiology **173**, 1763–1782.

Cardoso AA, Batz TA, McAdam SAM. 2020. Xylem embolism resistance determines leaf mortality during drought in *Persea americana*. Plant Physiology **182**, 547–554.

Carminati A, Javaux M. 2020. Soil rather than xylem vulnerability controls stomatal response to drought. Trends in Plant Science **25**, 868–880.

Charrier G, Delzon S, Domec JC, *et al.* 2018. Drought will not leave your glass empty: low risk of hydraulic failure revealed by long-term drought observations in world's top wine regions. Science Advances **4**, 1–10.

Chatelet DS, Matthews MA, Rost TL. 2006. Xylem structure and connectivity in grapevine (*Vitis vinifera*) shoots provides a passive mechanism for the spread of bacteria in grape plants. Annals of Botany **98**, 483–494.

Choat B, Drayton WM, Brodersen C, Matthews MA, Shackel KA, Wada H, McElrone AJ. 2010. Measurement of vulnerability to water stress-induced cavitation in grapevine: a comparison of four techniques applied to a long-vesseled species. Plant, Cell & Environment **33**, 1502–1512.

Christman MA, Sperry JS, Adler FR. 2009. Testing the 'rare pit' hypothesis for xylem cavitation resistance in three species of Acer. New Phytologist **182**, 664–674.

Christman MA, Sperry JS, Smith DD. 2012. Rare pits, large vessels and extreme vulnerability to cavitation in a ring-porous tree species. New Phytologist **193**, 713–720.

Cochard H, Venisse JS, Barigah TS, Brunel N, Herbette S, Guilliot A, Tyree MT, Sakr S. 2007. Putative role of aquaporins in variable hydraulic conductance of leaves in response to light. Plant Physiology **143**, 122–133.

Corso D, Delzon S, Lamarque LJ, Cochard H, Torres-Ruiz JM, King A, Brodribb TJ. 2020. Neither xylem collapse, cavitation or changing leaf conductance drive stomatal closure in wheat. Plant, Cell & Environment **43**, 854–865.

Cuneo IF, Knipfer T, Brodersen CR, McElrone AJ. 2016. Mechanical failure of fine root cortical cells initiates plant hydraulic decline during drought. Plant Physiology **172**, 1669–1678.

Diffenbaugh NS, Scherer M. 2013. Using climate impacts indicators to evaluate climate model ensembles: temperature suitability of premium winegrape cultivation in the United States. Climate Dynamics **40**, 709–729.

Galmés J, Pou A, Alsina MM, Tomàs M, Medrano H, Flexas J. 2007. Aquaporin expression in response to different water stress intensities and recovery in Richter-110 (*Vitis* sp.): relationship with ecophysiological status. Planta **226**, 671–681.

Hannah L, Roehrdanz PR, Ikegami M, Shepard AV, Shaw MR, Tabor G, Zhi L, Marquet PA, Hijmans RJ. 2013. Climate change, wine, and conservation. Proceedings of the National Academy of Sciences, USA **110**, 6907–6912.

Hernandez-Santana V, Rodriguez-Dominguez CM, Fernández JE, Diaz-Espejo A. 2016. Role of leaf hydraulic conductance in the regulation of stomatal conductance in almond and olive in response to water stress. Tree Physiology **36**, 725–735.

Hochberg U, Albuquerque C, Rachmilevitch S, Cochard H, David-Schwartz R, Brodersen CR, McElrone AJ, Windt CW. 2015*a*. Grapevine petioles are more sensitive to drought induced embolism than stems: evidence from *in vivo* MRI and microCT observations of hydraulic vulnerability segmentation. Plant, Cell & Environment **39**, 1886–1894.

Hochberg U, Bonel AG, David-Schwartz R, Degu A, Fait A, Cochard H, Peterlunger E, Herrera JC. 2017*b*. Grapevine acclimation to water deficit: the adjustment of stomatal and hydraulic conductance differs from petiole embolism vulnerability. Planta **245**, 1091–1104.

Hochberg U, Degu A, Gendler T, Fait A, Rachmilevitch S. 2015*b*. The variability in the xylem architecture of grapevine petiole and its contribution to hydraulic differences. Functional Plant Biology: FPB **42**, 357–365.

Hochberg U, Degu A, Toubiana D, Gendler T, Nikoloski Z, Rachmilevitch S, Fait A. 2013. Metabolite profiling and network analysis reveal coordinated changes in grapevine water stress response. BMC Plant Biology **13**, 1–16.

Hochberg U, Ponomarenko A, Zhang YJ, Rockwell FE, Holbrook NM. 2019. Visualizing embolism propagation in gas-injected leaves. Plant Physiology **180**, 874–881.

Hochberg U, Windt CW, Ponomarenko A, Zhang YJ, Gersony J, Rockwell FE, Holbrook NM. 2017*a*. Stomatal closure, basal leaf embolism, and shedding protect the hydraulic integrity of grape stems. Plant Physiology **174**, 764–775.

Holbrook NM, Ahrens ET, Burns MJ, Zwieniecki MA. 2001. In vivo observation of cavitation and embolism repair using magnetic resonance imaging. Plant Physiology **126**, 27–31.

Jacobsen AL, Pratt RB. 2012. No evidence for an open vessel effect in centrifuge-based vulnerability curves of a long-vesselled liana (*Vitis vinifera*). New Phytologist **194**, 982–990.

John GP, Scoffoni C, Sack L. 2013. Allometry of cells and tissues within leaves. American Journal of Botany **100**, 1936–1948.

Johnson DM, McCulloh KA, Woodruff DR, Meinzer FC. 2012. Evidence for xylem embolism as a primary factor in dehydration-induced declines in leaf hydraulic conductance. Plant, Cell & Environment **35**, 760–769.

Johnson DM, Meinzer FC, Woodruff DR, McCulloh KA. 2009. Leaf xylem embolism, detected acoustically and by cryo-SEM, corresponds to decreases in leaf hydraulic conductance in four evergreen species. Plant, Cell & Environment **32**, 828–836.

Kim YX, Steudle E. 2007. Light and turgor affect the water permeability (aquaporins) of parenchyma cells in the midrib of leaves of *Zea mays*. Journal of Experimental Botany **58**, 4119–4129.

Knipfer T, Cuneo IF, Brodersen CR, McElrone AJ. 2016. In situ visualization of the dynamics in xylem embolism formation and removal in the absence of root pressure: a study on excised grapevine stems. Plant Physiology **171**, 1024–1036.

Lersten NR. 1997. Occurrence of endodermis with a Casparian strip in stem and leaf. Botanical Review **63**, 265–272.

Levin A, Williams LE, Matthews M. 2019. A continuum of stomatal responses to water deficits among 17 wine grape cultivars (*Vitis vinifera*). Functional Plant Biology **47**, 11–25.

Lovisolo C, Perrone I, Hartung W, Schubert A. 2008. An abscisic acid-related reduced transpiration promotes gradual embolism repair when grapevines are rehydrated after drought. New Phytologist **180**, 642–651.

Martorell S, Medrano H, Tomàs M, Escalona JM, Flexas J, Diaz-Espejo A. 2015. Plasticity of vulnerability to leaf hydraulic dysfunction during acclimation to drought in grapevines: an osmotic-mediated process. Physiologia Plantarum **153**, 381–391.

Martre P, Morillon R, Barrieu F, North GB, Nobel PS, Chrispeels MJ. 2002. Plasma membrane aquaporins play a significant role during recovery from water deficit. Plant Physiology **130**, 2101–2110.

McElrone AJ, Brodersen CR, Alsina MM, Drayton WM, Matthews MA, Shackel KA, Wada H, Zufferey V, Choat B. 2012. Centrifuge technique consistently overestimates vulnerability to water stress-induced cavitation in grapevines as confirmed with high-resolution computed tomography. New Phytologist **196**, 661–665.

Mertz RA, Brutnell TP. 2014. Bundle sheath suberization in grass leaves: multiple barriers to characterization. Journal of Experimental Botany **65**, 3371–3380.

Morales-Castilla I, García de Cortázar-Atauri I, Cook BI, Lacombe T, Parker A, van Leeuwen C, Nicholas KA, Wolkovich EM. 2020. Diversity buffers winegrowing regions from climate change losses. Proceedings of the National Academy of Sciences, USA **117**, 2864–2869.

Nardini A, Salleo S, Raimondo F. 2003. Changes in leaf hydraulic conductance correlate with leaf vein embolism in *Cercis siliquastrum* L. Trees - Structure and Function **17**, 529–534.

Nardini A, Tyree MT, Salleo S. 2001. Xylem cavitation in the leaf of *Prunus laurocerasus* and its impact on leaf hydraulics. Plant Physiology **125**, 1700–1709.

Pantin F, Monnet F, Jannaud D, Costa JM, Renaud J, Muller B, Simonneau T, Genty B. 2013. The dual effect of abscisic acid on stomata. New Phytologist **197**, 65–72.

Pou A, Medrano H, Flexas J, Tyerman SD. 2013. A putative role for TIP and PIP aquaporins in dynamics of leaf hydraulic and stomatal conductances in grapevine under water stress and re-watering. Plant, Cell & Environment **36**, 828–843.

Rockwell FE, Holbrook NM, Stroock AD. 2014. The competition between liquid and vapor transport in transpiring leaves. Plant Physiology **164**, 1741–1758.

Sack L, Cowan PD, Holbrook NM. 2003. The major veins of mesomorphic leaves revisited: tests for conductive overload in *Acer saccharum* (Aceraceae) and *Quercus rubra* (Fagaceae). American Journal of Botany **90**, 32–39.

Sack L, Holbrook NM. 2006. Leaf hydraulics. Annual Review of Plant Biology **57**, 361–381.

Sack L, Melcher PJ, Zwieniecki MA, Holbrook NM. 2002. The hydraulic conductance of the angiosperm leaf lamina: a comparison of three measurement methods. Journal of Experimental Botany **53**, 2177–2184.

Sack L, Pasquet-Kok J; PrometheusWiki contributors. 2011. Leaf pressure–volume curve parameters. 2011. PrometheusWiki. Available at: tiki-pagehistory.php?page=Leaf pressure-volume curve parameters&preview=16

Sack L, Scoffoni C. 2012. Measurement of leaf hydraulic conductance and stomatal conductance and their responses to irradiance and dehydration using the Evaporative Flux Method (EFM). Journal of Visualized Experiments (70), 4179.

Sade N, Shatil-Cohen A, Attia Z, Maurel C, Boursiac Y, Kelly G, Granot D, Yaaran A, Lerner S, Moshelion M. 2014. The role of plasma membrane aquaporins in regulating the bundle sheath–mesophyll continuum and leaf hydraulics. Plant Physiology **166**, 1609–1620.

Sade N, Shatil-Cohen A, Moshelion M. 2015. Bundle-sheath aquaporins play a role in controlling *Arabidopsis* leaf hydraulic conductivity. Plant Signaling & Behavior **10**, 1–4.

Salleo S, Nardini A, Pitt F, Lo Gullo MA. 2000. Xylem cavitation and hydraulic control of stomatal conductance in Laurel (*Laurus nobilis* L.). Plant, Cell &Environment **23**, 71–79.

Schultz HR. 2003. Differences in hydraulic architecture account for near-isohydric and anisohydric behaviour of two field-grown *Vitis vinifera* L. cultivars during drought. Plant, Cell & Environment **26**, 1393–1405.

Scoffoni C, Albuquerque C, Brodersen CR, Townes SV, John GP, Bartlett MK, Buckley TN, McElrone AJ, Sack L. 2017*b*. Outside-xylem vulnerability, not xylem embolism, controls leaf hydraulic decline during dehydration. Plant Physiology **173**, 1197–1210.

Scoffoni C, Albuquerque C, Brodersen CR, Townes SV, John GP, Cochard H, Buckley TN, McElrone AJ, Sack L. 2017*a*. Leaf vein xylem conduit diameter influences susceptibility to embolism and hydraulic decline. New Phytologist **213**, 1076–1092.

Scoffoni C, Albuquerque C, Cochard H, *et al.* 2018. The causes of leaf hydraulic vulnerability and its influence on gas exchange in *Arabidopsis thaliana*. Plant Physiology **178**, 1584–1601.

Scoffoni C, McKown AD, Rawls M, Sack L. 2012. Dynamics of leaf hydraulic conductance with water status: quantification and analysis of species differences under steady state. Journal of Experimental Botany **63**, 643–658.

Scoffoni C, Rawls M, McKown A, Cochard H, Sack L. 2011. Decline of leaf hydraulic conductance with dehydration: relationship to leaf size and venation architecture. Plant Physiology **156**, 832–843.

Scoffoni C, Sack L. 2017. The causes and consequences of leaf hydraulic decline with dehydration. Journal of Experimental Botany **68**, 4479–4496.

Shatil-Cohen A, Attia Z, Moshelion M. 2011. Bundle-sheath cell regulation of xylem–mesophyll water transport via aquaporins under drought stress: a target of xylem-borne ABA? The Plant Journal **67**, 72–80.

Shelden MC, Vandeleur R, Kaiser BN, Tyerman SD. 2017. A comparison of petiole hydraulics and aquaporin expression in an anisohydric and isohydric cultivar of grapevine in response to water-stress induced cavitation. Frontiers in Plant Science **8**, 1–17.

Skelton RP, Brodribb TJ, Choat B. 2017. Casting light on xylem vulnerability in an herbaceous species reveals a lack of segmentation. New Phytologist **214**, 561–569.

Smith R, Prichard T. 2002. Using a pressure chamber in winegrapes. UC Cooperative Extension. http://cesonoma.ucdavis.edu/files/27409.pdf

Taneda H, Kandel DR, Ishida A, Ikeda H. 2016. Altitudinal changes in leaf hydraulic conductance across five Rhododendron species in eastern Nepal. Tree Physiology **36**, 1272–1282.

Thorne ET, Young BM, Young GM, Stevenson JF, Labavitch JM, Matthews MA, Rost TL. 2006. The structure of xylem vessels in grapevine (Vitaceae) and a possible passive mechanism for the systemic spread of bacterial disease. American Journal of Botany **93**, 497–504.

Torres-Ruiz JM, Jansen S, Choat B, *et al.* 2015. Direct x-ray microtomography observation confirms the induction of embolism upon xylem cutting under tension. Plant Physiology **167**, 40–43.

Trifilò P, Gascó A, Raimondo F, Nardini A, Salleo S. 2003*a*. Kinetics of recovery of leaf hydraulic conductance and vein functionality from cavitation-induced embolism in sunflower. Journal of Experimental Botany **54**, 2323–2330.

Trifilò P, Nardini A, Lo Gullo MA, Salleo S. 2003*b*. Vein cavitation and stomatal behaviour of sunflower (*Helianthus annuus*) leaves under water limitation. Physiologia Plantarum **119**, 409–417.

Trifiló P, Raimondo F, Savi T, Lo Gullo MA, Nardini A. 2016. The contribution of vascular and extra-vascular water pathways to drought-induced decline of leaf hydraulic conductance. Journal of Experimental Botany **67**, 5029–5039.

Tyree MT, Ewers FW. 1991. The hydraulic architecture of trees and other woody plants. New Phytologist **119**, 345–360.

Vandeleur RK, Mayo G, Shelden MC, Gilliham M, Kaiser BN, Tyerman SD. 2009. The role of plasma membrane intrinsic protein aquaporins in water transport through roots: diurnal and drought stress responses reveal different strategies between isohydric and anisohydric cultivars of grapevine. Plant Physiology **149**, 445–460.

Wang X, Du T, Huang J, Peng S, Xiong D. 2018. Leaf hydraulic vulnerability triggers the decline in stomatal and mesophyll conductance during drought in rice. Journal of Experimental Botany **69**, 4033–4045.

Williams LE, Araujo FJ. 2002. Correlations among predawn leaf, midday leaf, and midday stem water potential and their correlations with other measures of soil and plant water status in *Vitis vinifera*. Journal of the American Society of Horticultural Science **127**, 448–454.

Williams LE, Baeza P. 2007. Relationships among ambient temperature and vapor pressure deficit and leaf and stem water potentials of fully irrigated, field-grown grapevines. American Journal of Enology and Viticulture **58**, 173–181.

Zhang YJ, Rockwell FE, Graham AC, Alexander T, Holbrook NM. 2016. Reversible leaf xylem collapse: a potential 'circuit breaker' against cavitation. Plant Physiology **172**, 2261–2274.

Zufferey V, Cochard H, Ameglio T, Spring JL, Viret O. 2011. Diurnal cycles of embolism formation and repair in petioles of grapevine (*Vitis vinifera* cv. Chasselas). Journal of Experimental Botany **62**, 3885–3894.